Supporting Information

Inhibiting Excessive Molecular Aggregation to Achieve Highly Efficient and Stabilized Organic Solar Cells by Introducing Star-Shaped Nitrogen Heterocyclic-Ring Acceptor

Xunfan Liao,[a†] Qian Xie,[a,b†] Yaxiao Guo,[c†] Qiannan He,[b] Zeng Chen,[d] Na Yu,[e] Peipei Zhu,[a] Zaifei Ma,[e] Yongjie Cui,[a,e] Xiaobao Xu,[f] Haiming Zhu[d] and Yiwang Chen[a,b]*

Prof. X. Liao, Mr. Q. Xie, Dr. P. Zhu, Mr. Y. Cui, Prof. Y. Chen
[a]Institute of Advanced Scientific Research (iASR), Key Laboratory of Functional Small Molecules for Ministry of Education, Jiangxi Normal University, 99 Ziyang Avenue, Nanchang 330022, China.
ywchen@ncu.edu.cn

Mr. Q. Xie, Mrs. Q. He, Prof. Y. Chen
[b]College of Chemistry/Institute of Polymers and Energy Chemistry (IPEC), Nanchang University, 999 Xuefu Avenue, Nanchang 330031, China

Prof. Y. Guo
[c]State Key Laboratory of Separation Membranes and Membrane Processes, School of Chemistry, Tiangong University, Tianjin 300387, China

Mr. Z. Chen, Prof. H. Zhu
[d]Center for Chemistry of High-Performance & Novel Materials, Department of Chemistry, Zhejiang University, Hangzhou 310027, China

Mrs. N. Yu, Mr. Y. Cui, Prof. Z. Ma
[e]State Key Laboratory for Modification of Chemical Fibers and Polymer Materials, Center for Advanced Low-dimension Materials, College of Materials Science and Engineering, Donghua University, Shanghai, 201620, P. R. China

Prof. X. Xu
[f]School of Materials Science and Engineering, Nanjing University of Science and Technology, Nanjing 210094, China

Experimental Section

Materials. All the starting materials were purchased from commercial suppliers and used without further purification. PM6, Y6 and PDINO were purchased from Solarmer Materials Inc. Indium-tin oxide (ITO) glass was gained from South China Science & Technology Company Limited, whereas PEDOT:PSS (Clevios P VP Al4083) was obtained from Heraeus. 1-chloronaphthalene (1-CN), chloroform was purchased from Sigma-Aldrich Inc. Al was obtained from Zhong Nuo Advanced Material Technology CO Limited.

Device fabrication.

BHJ structure devices: The device structure is ITO/PEDOT:PSS/active layers/PDINO/Al. The ITO glass was gradually washed by acetone, deionized water, and isopropyl alcohol for 20 min in the ultrasonic wave cleaning machine, respectively. Then, the ITO glass was treated with 3 min air plasma (Plasma Cleaner PPC862) after drying by nitrogen gun. After that, PEDOT:PSS was spin-coated onto the ITO substrate at 4000 rpm for 50 s, and the PEDOT:PSS layer was annealed at 150 °C for 15 min in an ambient atmosphere. Then, the devices were transferred to the glovebox. The donor:acceptor (D:A) blend solution was spin-casted at 3000 rpm for 50 s. The D/A blends were dissolved in CF (16 mg mL^{-1}, total D/A is 1/1.2) with 0.5% CN (volume fraction). Subsequently, the active layer was treated with thermal annealing at 100 °C for 10 min. PDINO was dissolved in methanol (1 mg mL^{-1}), which was spin-coated at 3000 rpm for 50 s. Finally, the 100 nm Al layer was deposited as the top electrode under high vacuum (≈3 × 10^{-4} Pa), and the device was completed. In addition, the BHJ structure ternary devices were also fabricated by this way.

PPHJ structure devices: The device structure is ITO/PEDOT:PSS/PM6/Y6:TF1/PDINO/Al. The ITO glass was gradually washed by acetone, deionized water, and isopropyl alcohol for 20 min in the ultrasonic wave cleaning machine, respectively. Then, the ITO glass was treated with 3 min air plasma (Plasma Cleaner PPC862) after drying by nitrogen gun. After that, PEDOT:PSS was

spin-coated onto the ITO substrate at 4000 rpm for 50 s, and the PEDOT:PSS layer was annealed at 150 °C for 15 min in an ambient atmosphere. Then, the devices were transferred to the glovebox. The neat PM6 in CB solution (10 mg mL^{-1}) was spin-coated onto the PEDOT:PSS-coated substrates, and then Y6:TF1 in CF solution (10 mg mL^{-1}) with 0.5% CN (volume fraction) was subsequently spin-coated (at 2000 r.p.m.) on top of PM6 layer, thermal-annealing was used after the spin-coating of the acceptor layer at 100 °C for 10 min. PDINO was dissolved in methanol (1 mg mL^{-1}), which was spin-coated at 3000 rpm for 50 s. Finally, the 100 nm Al layer was deposited as the top electrode under high vacuum (≈3 × 10^{-4} Pa), and the device was completed.

Instruments and Measurement

Optical characterizations. The current−voltage (*J-V*) characteristics were measured by a Keithley 2400 Source Meter under simulated solar light (100 mW/cm^2, AM 1.5 G, Abet Solar Simulator Sun2000). The EQE spectra were recorded on a commercial EQE measurement system (Enlitech, QE-R3011). UV-vis absorption spectra were recorded on a Perkin Elmer Lambda 750 spectrophotometer.

Electrochemical characterizations. Cyclic voltammetry (CV) was performed by a Zahner IM6e electrochemical working station, using Ag/AgCl as the reference electrode, a Pt plate as the counter electrode, and a glassy carbon as the working electrode. The acceptors were drop-cast onto the electrode from chloroform solutions to form thin films. 0.1 mol/L tetrabutylammonium hexafluorophosphate in anhydrous acetonitrile was used as the supporting electrolyte. The scan rate was 0.05 V/s. The E_{HOMO} and E_{LUMO} are calculated as refer to the equations of E_{HOMO} = - (E_{ox}+4.4) eV and E_{LUMO} = - (E_{red}-4.4) eV.

Density functional theory (DFT) calculation

The molecuar structures were optimized with a functional of B3LYP and a basis set of 6-31G(d,p). The alkyl chians were replaced by methyl for saving computation time.

The ESP analysis was carried out by a wavefunction analysis tool Multiwfn. The surface electrostatic potential (ESP) distribution diagrams of the non-fullerene acceptors were simulated with an electron density of 0.001 a.u. Molecular polarity index (MPI) of the acceptor molecules were calculated on the basis of the distribution characteristics of the ESP on the molecular surface. The value of MPI can be given through the following formula:

$$MPI = (1/A)\iint_S |V(r)|dS$$

where V is the electrostatic potential of the molecule, integration is the integration of the molecular surface S, and A is the molecular surface area. The greater the MPI, the greater the overall polarity of the molecule. Because the nonuniformity of the charge distribution in the system is a manifestation of the polarity of the molecules, the more uneven the distribution, the more positive or negative regions of the electrostatic potential on the surface of the molecule will appear, making the MPI larger. The molecular polar surface area is the area where the absolute value of the ESP is greater than 10 kcal/mol, and the molecular non-polar surface area is the area where the absolute value of the ESP is less than 10 kcal/mol.

Surface energy characterization. Contact angle measurements of films were performed at a Krüss DSA100s Drop Shape Analyzer. Water (72.8 mN m^{-1}, 25 °C) was used as probe liquids. The interfacial surface energy values of materials can be obtained directly by instrument, and it also according to Young's equation.

Hole and electron mobility measurements.

The device structure of ITO/PEDOT:PSS/active layer/MoO_3 /Ag and ITO/ZnO/active layer/PDNIO/Ag was employed to fabricate the hole-only and electron-only diodes, respectively. The carrier mobilities were measured using the space-charge-limited-current (SCLC) model, which is described by:

$$J = 9\varepsilon_0\varepsilon_r u V^2/8L^3$$

where J is the current density, L is the film thickness of active layer, ε_0 is the permittivity of free space (8.85×10^{-12} F m^{-1}), εr is the relative dielectric constant of the transport medium, u is the hole or electron mobility, V is the internal voltage in the device and $V = V_{appl}-V_r-V_{bi}$, where V_{appl} is the applied voltage to the device, V_r is the voltage drop due to contact resistance and series resistance across the electrodes, and V_{bi} is the built-in voltage due to the relative work function difference of the two electrodes. The hole-mobility can be calculated from the slope of the $J^{1/2}\sim V$ curves.

Sensitive EQE Measurement. A 150 W quartz halogen lamp (LSH-75, Newport) acted as a light source, passing through the monochromator (CS260-RG-3-MC-A, Newport) to provide an adjustable monochromatic light source for testing, and then emited an optical signal at a 173 Hz frequency through the chopper (3502 Optical Chopper, Newport) and focused on the OSC devices. The current generated by the device was amplified by the front-end current amplifier (SR570, Stanford) to reduce the impact of the noise signal. The final signal was collected and analyzed by a Phase-locked Amplifier (SR830 DSP Lock-In Amplifier, Stanford).

EL Measurement. EL measurement was conducted by direct-current meter (PWS2326, Tectronix) to provide bias voltage for the test device, and the EL spectra were recorded by the fluorescence spectrometer (KYMERA-328I-B2, Andor technology LTD) with cooled silicon array and indium gallium arsenic detector, which was calibrated by standard light source (Ocean Optics).

EQE_{EL} Measurement. The EQE_{EL} was recorded with an in-house-built system comprising a standard silicon photodiode (S1337-1010BR, Hamamatsu Electronics), Keithley 2400 source meter (for supplying voltages and recording injected currents), and Keithley 6482 picoammeter (for measuring the emitted light intensity).

AFM characterizations. The morphologies of active layers were investigated by Bruker Multimode 8 high resolution scanning probe microscope. The specimen for

AFM measurements was prepared using the same procedures those for fabricating devices but without PDINO/Al on top of the active layer.

GIWAXS characterization. GIWAXS measurement were carried out with a Xeuss 2.0 SAXS/WAXS laboratory beamline using a Cu X-ray source (8.05 keV, 1.54 Å) and a Pilatus 3R 300K detector. The incidence angle is 0.2°. The samples for GIWAXS measurements are fabricated on silicon substrates using the same recipe for the devices but without PDINO/Al on top of the active layer.

DSC measurements. DSC was measured by TA DSC Q2000 differential scanning calorimeter, with the samples being heated to 200 °C and then cooled to 40 °C at a heating/cooling rate of 10 °C/min.

XPS profiling. X-ray photoelectron spectroscopy (XPS, Thermo Scientific ESCALAB 250Xi) was used for binding energy and element distribution analysis. The XPS was measured in the high vacuum stage, about 1×10^{-10} Pa. And all XPS spectra were calibrated by setting the peak corresponding to aliphatic carbon to 284.8 eV. Samples for XPS were prepared using the same methods for the active layer for the organic photovoltaics.

Confocal polarization PL microscopy and lifetimes of PL measurements. The confocal polarization PL microscopy and lifetimes of PL were detected by PL 1 system by ISS (Champaign, IIIinois, USA). The specimen for PL measurements was prepared using the same procedures those for fabricating devices but without PDINO/Al on top of the active layer. For PL measurements, a (375 nm) laser is pulsed at 200 MHz and attenuated using a variable ND filter wheel and then coupled into the confocal microscope using a single mode fiber.

Transient absorption spectroscopy (TAS). For femtosecond transient absorption spectroscopy, the fundamental output from Yb:KGW laser (1030 nm, 220 fs Gaussian

fit, 100 kHz, Light Conversion Ltd) was separated to two light beam. One was introduced to NOPA (ORPHEUS-N, Light Conversion Ltd) to produce a certain wavelength for pump beam (here we use 750 nm, 30 fs pulse duration), the other was focused onto a YAG plate to generate white light continuum as probe beam. The pump and probe overlapped on the sample at a small angle less than 10. The transmitted probe light from sample was collected by a linear CCD array.

Supporting Figures and Tables

Table S1. Photovoltaic parameters for reported PPHJ structure-based OSCs devices.

Active layer	*Voc* (V)	FF	*J*sc (mA cm^{-2})	PCE (%)	References
PBDB-T/ITIC	0.82	0.63	19.45	10.04	1
J71/ITCPTC	0.91	0.63	18.21	10.44	2
J71/ITIC	0.93	0.65	17.98	10.94	2
J71/ITC6-IC	0.97	0.70	16.85	11.47	3
PTFB-O/ITIC-Th	0.91	0.74	17.50	11.80	4
PBDB-T:FOIC/PBDB-T:IT-M	0.75	0.64	24.66	11.86	5
PTB7-Th/FOIC1	0.70	0.72	23.80	12.0	6
PffBT4T-2OD/IEICO-4F	0.71	0.71	20.90	10.60	7
J71/ITC6-IC	0.98	0.66	18.57	12.08	2
PTB7-Th/FOIC:N2200	0.73	0.73	24.36	12.27	8
FTAZ/IT-M	0.96	0.70	18.30	12.30	9
PTQ10/IDIC	0.94	0.70	18.75	12.32	2
PM6/IT-4F	0.84	0.75	20.50	12.90	10
PBDB-TFS1/IT-4F	0.90	0.71	20.30	13.0	11
PM6/IT-4F	0.85	0.74	20.81	13.19	12
PM6/IT4F:ICBA	0.88	0.75	21.25	15.30	12
PM6/IT-4F(DIO)	0.86	0.76	20.98	13.70	13
P2F-EHp/M4-4F	0.83	0.67	25.56	14.21	14
PM6/IT4F:F8IC	0.79	69.8	25.60	14.20	15
PM6/Y6	0.83	0.76	25.90	16.35	16
PT2/Y6	0.83	0.74	26.70	16.50	17
PM6/Y6	0.82	0.76	26.30	16.50	18
D18/N3	0.83	0.75	26.71	16.58	19
D18/N3	0.83	0.72	25.53	15.32	19
PM6/BO-4Cl	0.85	0.75	26.81	17.11	20
PM6/BTP-S2	0.94	0.73	21.98	15.04	20
PM6/Y6-BO	0.84	0.74	26.10	16.20	21
PNBT-Cl/N3	0.86	0.73	24.46	15.23	22
PM6/Y6:TF1	**0.87**	**0.75**	**25.89**	**16.91**	**This work**

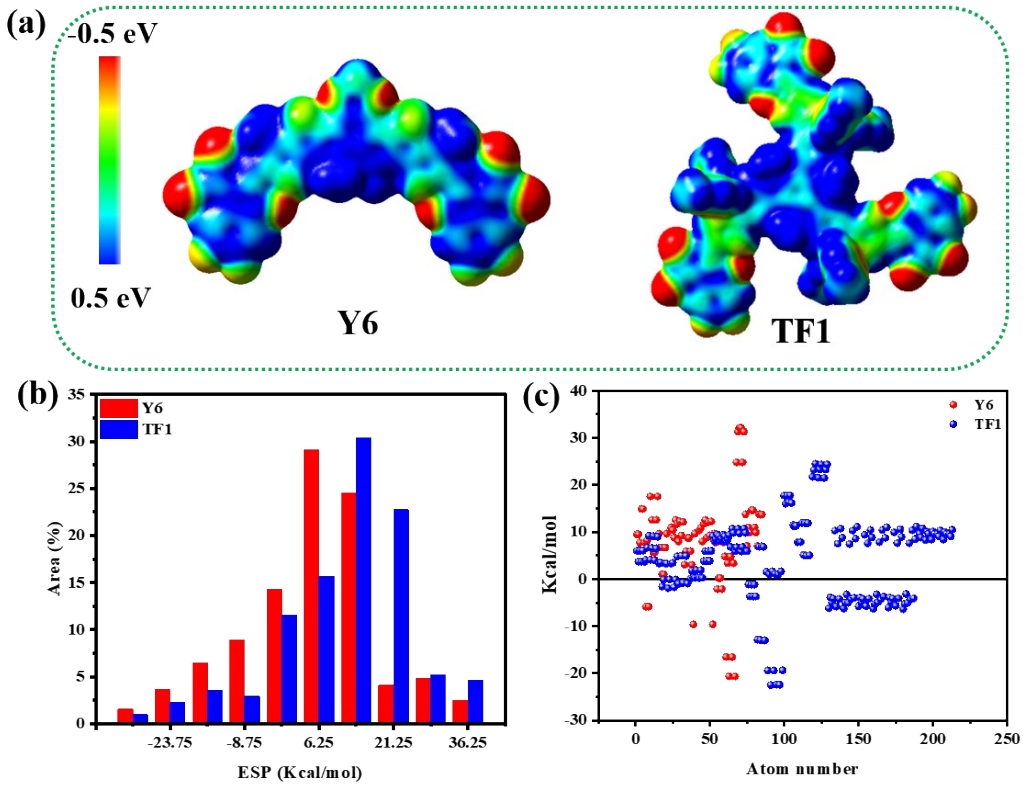

Figure S1. (a) The electrostatic potential (ESP) distribution maps of Y6 and TF1 and (b) the averaged ESP values of the surface area distribution and (c) each atom.

Table S2. Molecular surface area, MPI, extreme value of ESP and total average ESP of Y6 and TF1 (Isosurface = 0.001 au)

Acceptors	Overall surface area ($Å^2$)	MPI (Kcal/mol)	Minimal value (Kcal/mol)	Maximal value (Kcal/mol)	Overall average value (Kcal/mol)
Y6	807.44	11.70	-33.44	39.50	5.06
TF1	1752.76	10.23	-35.01	28.80	4.41

Substance	CA(L) [°]	CA(R) [°]	CA [°]	Surface energies [mN/m]
PM6	104.3	104.3	104.4	20.32
Y6	95.7	95.9	95.8	25.65
TF1	97.36	97.37	97.37	24.66

Table S3. The data of the contact angles (WCAs) of PM6, TF1 and Y6 films.

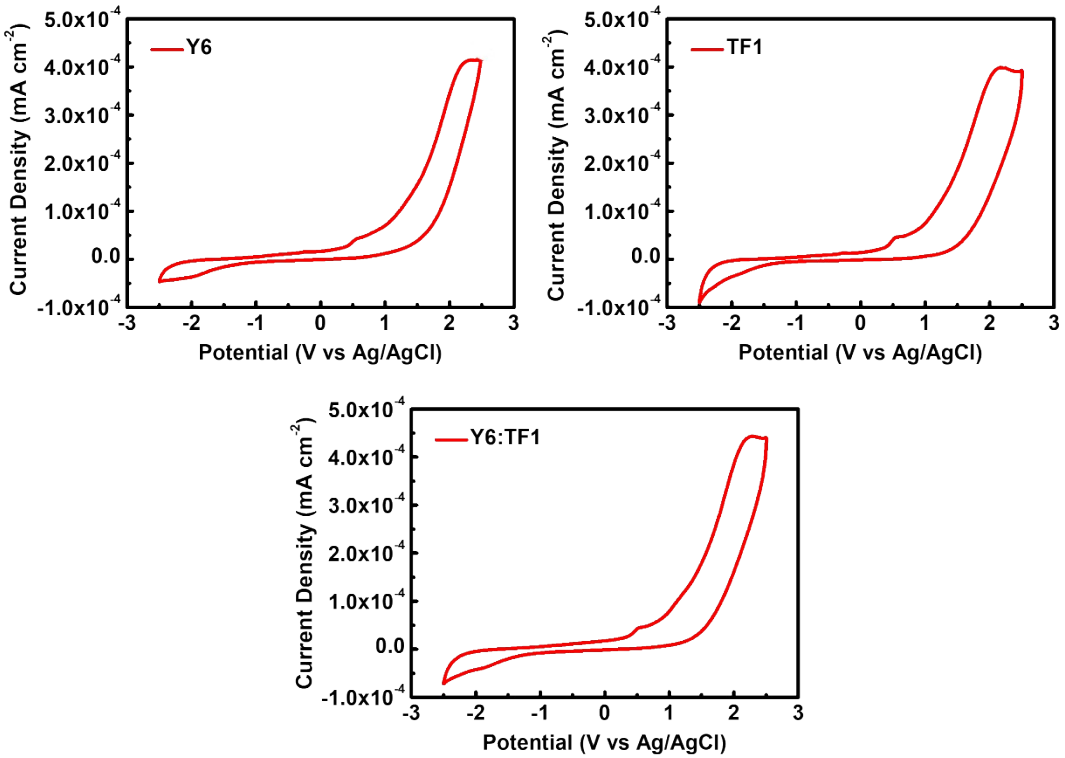

Figure S2. Cyclic voltammogram (CV) curve of Y6, TF1 and Y6:TF1 (1.1:0.1 wt %).

Table S4. Optical and electrochemical properties of Y6, TF1 and Y6:TF1 (1.1:0.1 wt %).

	λ_{oneset} [nm]	HOMO [eV]	LUMO [eV]	E_g^{opt} [eV]
Y6	948	-5.65	-4.34	1.31
Y6:TF1	921	-5.53	-4.18	1.35
TF1	850	-5.38	-3.92	1.46

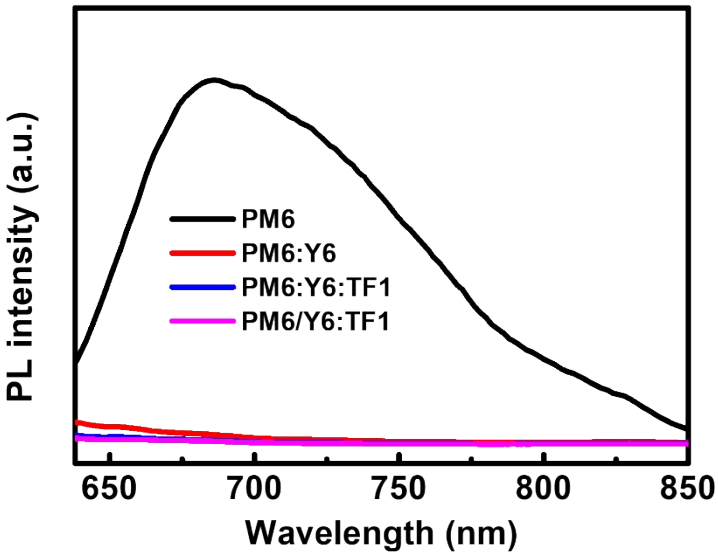

Figure S3. PL emission spectra of PM6 neat film and blended films.

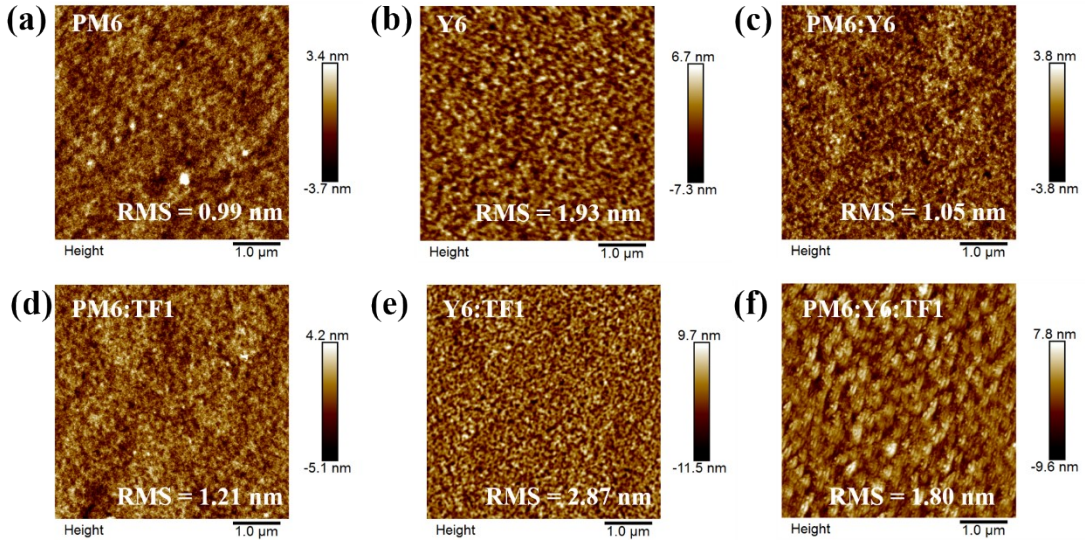

Figure S4. AFM height images of (a) PM6, (b) Y6, (c) PM6:Y6 (1:1.2 wt %), (d) PM6:TF1 (1:0.1 wt %), (e) Y6:TF1 (1.1:0.1 wt %) and PM6:Y6:TF1 (1:1.1:0.1 wt %).

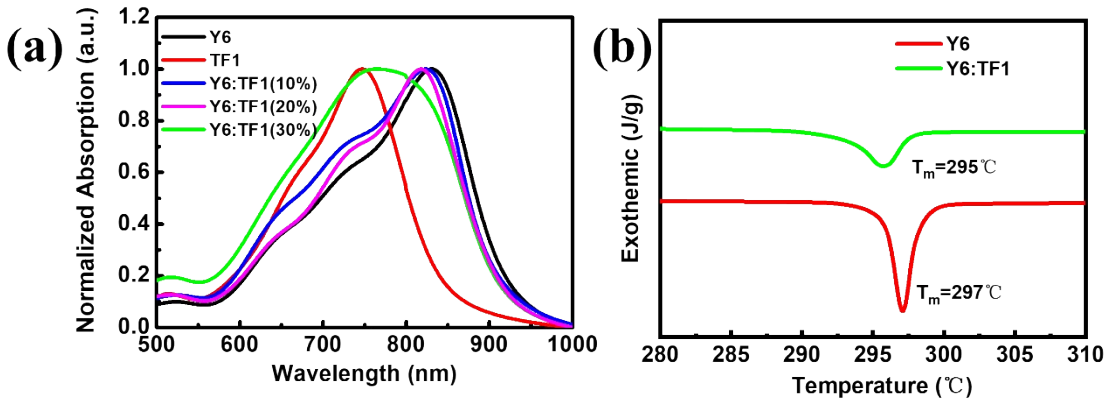

Figure S5. (**a**) The normalized UV-vis absorption spectra for the pure films of Y6, TF1 and the blend films of Y6:TF1 with different weight ratio and (**b**) differential scanning calorimetry (DSC) thermograms of Y6 and Y6:TF1 at 10 °C min^{-1}.

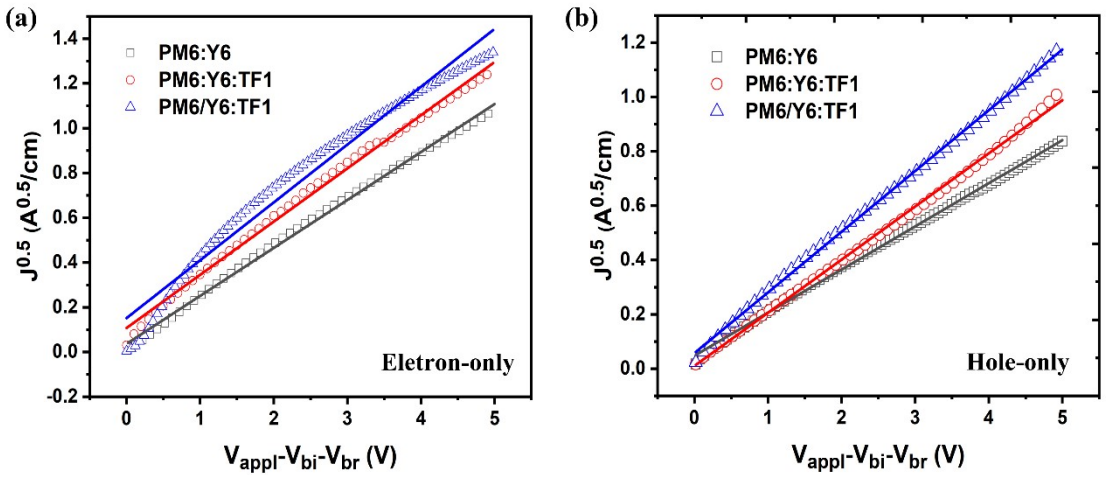

Figure S6. (a) $J^{0.5}-V$ plots of electron-only devices with a structure of ITO/ZnO/active layer/PDINO/Al. (b) $J^{0.5}-V$ plots of hole-only devices with a structure of ITO/PEDOT:PSS/ active layer/MoO_3/Ag.

Table S5. The electron and hole mobilities of the devices based on different blend films.

Device	μ_e ($\times10^{-4}$ cm^2 V^{-1} s^{-1})	μ_h ($\times10^{-4}$ cm^2 V^{-1} s^{-1})	μ_e/μ_h
PM6:Y6	1.99	1.14	1.75
PM6:Y6:TF1	2.59	1.73	1.50
PM6/Y6:TF1	3.04	2.24	1.36

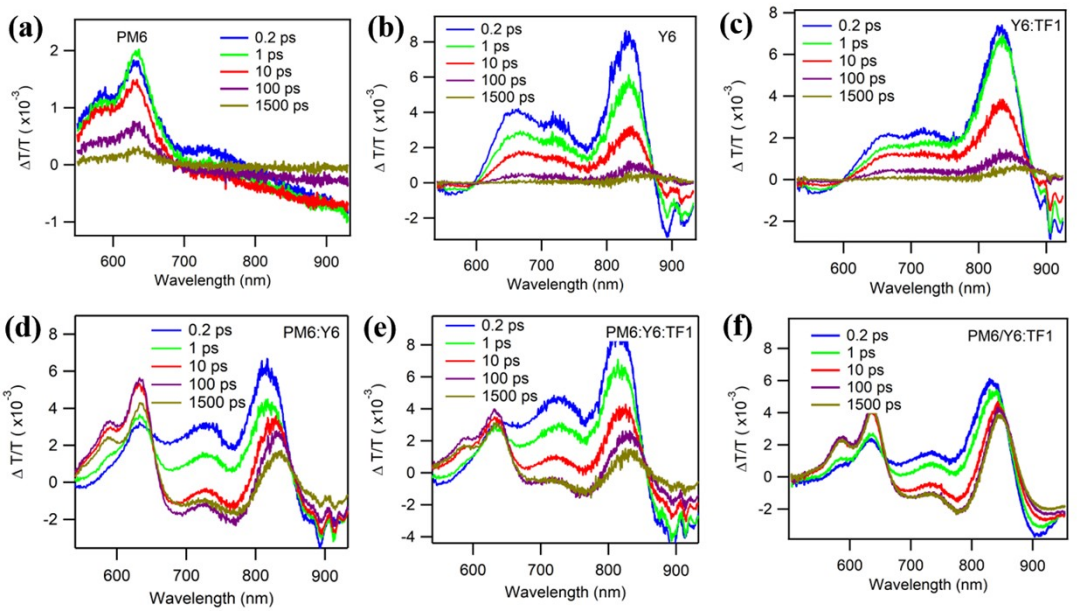

Figure S7. TA spectra of (a) PM6 under 550 nm excitation with a fluence below 5 μJ/cm^2, and (b) Y6, (c) Y6:TF1, (d) PM6:Y6, (e) PM6:Y6:TF1, (f) PM6/Y6:TF1 under 750 nm excitation with a fluence below 10 μJ/cm^2 at different delay times.

Table S6. The rising kinetics of PM6 GSB in binary and ternary blends.

Active layer	A_1	t_1 (ps)	A_2	t_2 (ps)
PM6:Y6	40.7%	0.161±0.016	59.3%	5.46±0.55
PM6:Y6:TF1	61.9%	0.127±0.013	38.1%	10.12±1.01
PM6/Y6:TF1	56.7%	0.118±0.012	43.2%	7.12±0.71

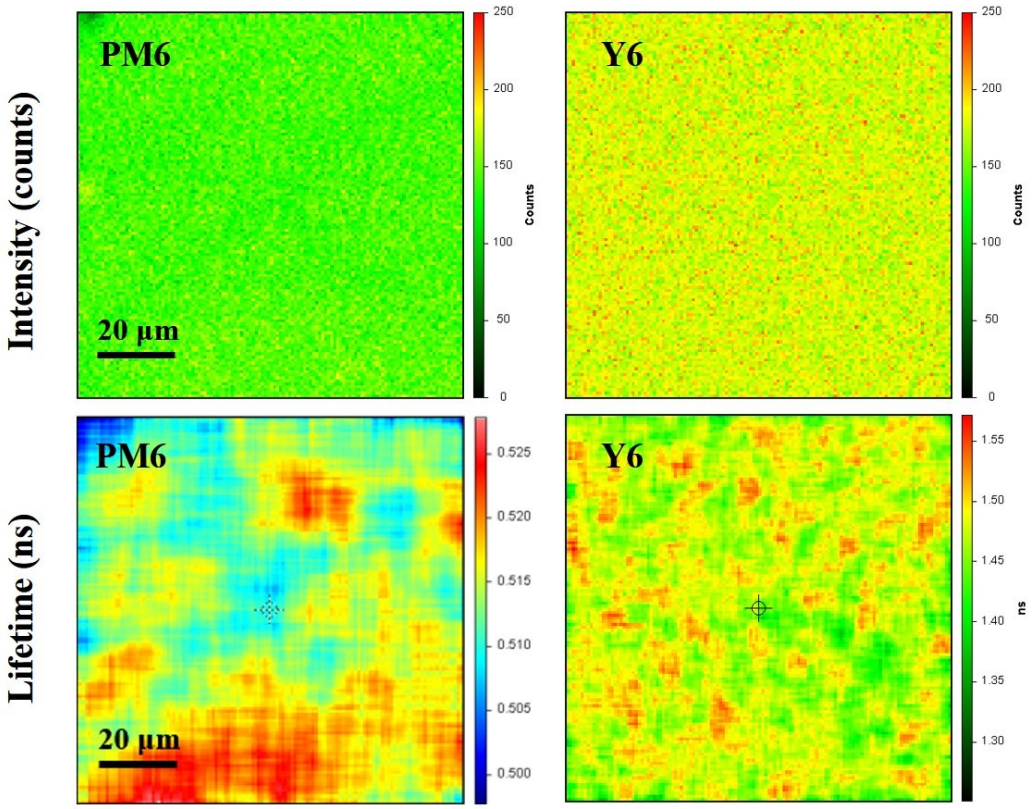

Figure S8. Photoluminescence results of PM6:Y6, PM6:Y6:TF1, PM6/Y6:TF1 (Top) and Lifetime imaging results of PM6:Y6, PM6:Y6:TF1, PM6/Y6:TF1 (Bottom).

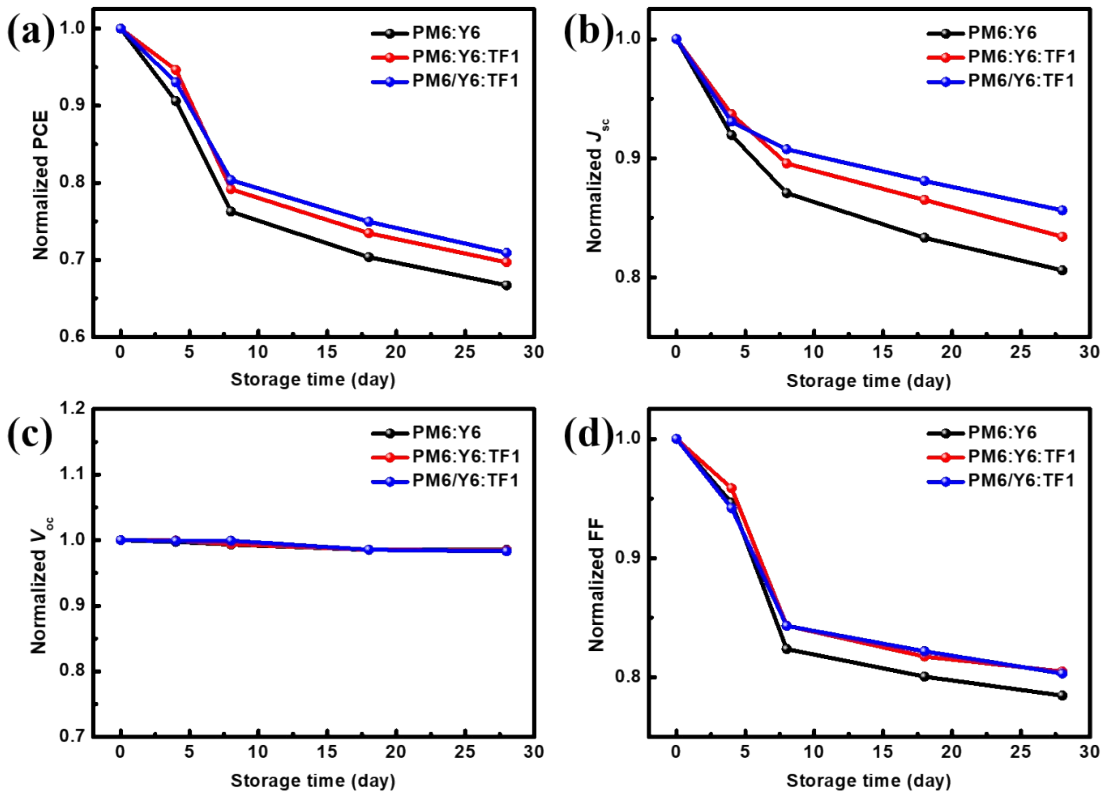

Figure S9. Normalized (a) PCE, (b) J_{sc}, (c) V_{oc}, (d) FF for storage lifetime of the binary device (PM6:Y6) and ternary device (PM6:Y6:TF1 and PM6/Y6:TF1) in a nitrogen-fill glovebox in the dark.

References:

[1] G. Xu, L. Chen, H. Lei, Z. Liao, N. Yi, J. Liu, Y. Chen, *J. Mater. Chem. A*, 2019, **7**, 4145-4152.

[2] R. Sun, J. Guo, C. Sun, T. Wang, Z. Luo, Z. Zhang, X. Jiao, W. Tang, C. Yang, Y. Li, J. Min, *Energy Environ. Sci.,* 2019,**12**, 384-395.

[3] R. Sun, J. Guo, Q. Wu, Z. Zhang, W. Yang, J. Guo, M. Shi, Y. Zhang, S. Kahmann, L. Ye, X. Jiao, M. A. Loi, Q. Shen, H. Ade, W. Tang, C. J. Brabec, J. Min, *Energy Environ. Sci.,* 2019, **12**, 3118.

[4] L. Arunagiri, G. Zhang, H. Hu, H. Yao, K. Zhang, Y. Li, P. C. Y. Chow, H. Ade, H. Yan, *Adv. Funct. Mater.,* 2019, **29**, 1902478

[5] Y. Wang, X. Wang, B. Lin, Z. Bi, X. Zhou, H. B. Naveed, K. Zhou, H. Yan, Z. Tang, W. Ma, *Adv. Energy Mater.*, **2020**, DOI: 10.1002/aenm.202000826.

[6] P. Xue, S. Dai, T.-K. Lau, J. Yu, J. Zhou, Y. Xiao, K. Meng, Z. Xie, G. Lu, X. Lu, R. P. S. Han, X. Zhan, *Sol. RRL.*, 2020, **4**, 2000115.

[7] K. Weng, L. Ye, L. Zhu, J. Xu, J. Zhou, X. Feng, G. Lu, S. Tan, F. Liu and Y. Sun, *Nat. Commun.,* 2020, **11**, 2855-2864.

[8] Y. Wang, Q. Zhu, H. B. Naveed, H. Zhao, K. Zhou, W. Ma, *Adv. Energy Mater.,* 2020, **10**, 1903609.

[9] L. Ye, Y. Xiong, Z. Chen, Q. Zhang, Z. Fei, R. Henry, M. Heeney, B. T. O'Connor, W. You, H. Ade, *Adv. Mater.,* 2019, **31**, 1808153.

[10] S. Dong, K. Zhang, B. Xie, J. Xiao, H-L. Yip, H.Yan, F. Huang, Y. Cao, *Adv. Energy Mater.,* 2019, **9**, 1802832.

[11] Y. Cui, S. Zhang, N. Liang, J. Kong, C. Yang, H. Yao, L. Ma, J. Hou, *Adv. Mater.,* 2018, **30**, 1802499.

[12] S. Liu, D. Chen, X. Hu, Z. Xing, J. Wan, L. Zhang, L. Tan, W. Zhou, Y. Chen, *Adv. Funct. Mater.,* 2020, **30**, 2003223.

[13] Q. He, W. Sheng, M. Zhang, G. Xu, P. Zhu, H. Zhang, Z. Yao, F. Gao, F. Liu, X. Liao, Y. Chen, *Adv. Energy Mater.* 2021, **11**, 2003390.

[14] D. Zhang, W. Zhong, L. Ying, B. Fan, M. Li, Z. Gan, Z. Zeng, D. Chen, N. Li, F. Huang, Y. Cao, *Nano Energy* 2021, DOI: 10.1016/j.nanoen.2021.105957.

[15] J. Wan, L. Zhang, Q. He, S. Liu, B. Huang, L. Hu, W. Zhou, Y. Chen, *Adv. Funct. Mater.,* 2020, **30**, 1909760.

[16] R. Sun, Q. Wu, J. Guo, T. Wang, Y. Wu, B. Qiu, Z. Luo, W. Yang, Z. Hu, J. Guo, M. Shi, C. Yang, F. Huang, Y. Li, J. Min, *Joule* 2020, **4**, 407.

[17] L. Zhan, S. Li, T-K. Lau, Y. Cui, X. Lu, M. Shi, C-Z. Li, H. Li, J. Hou, H. Chen, *Energy Environ. Sci.,* 2020,**13**, 635-645.

[18] Q. Li, L.-M. Wang, S. Liu, L. Guo, S. Dong, G. Ma, Z. Cao, X. Zhan, X. Gu, T. Zhu, Y.-P. Cai and F. Huang, *ACS Energy Lett.,* 2020, **5**, 3637-3646.

[19] Y. Wei, J. Yu, L. Qin, H. Chen, X. Wu, Z. Wei, X. Zhang, L. Ding, F. Gao, H. Huang, *Energy Environ. Sci.,* 2021, DOI: 10.1039/d0ee03490h.

[20] L. Zhan, S. Li, X. Xia, Y. Li, X. Lu, L. Zuo, M. Shi and H. Chen, *Adv. Mater.,* 2021, DOI: 10.1002/adma.202007231.

[21] H. Fu, W. Gao, Y. Li, F. Lin, X. Wu, J. H Son, J. Luo, H-Y. Woo, Z. Zhu, A. K.-Y. Jen, *Small Methods*, 2020, **4**, 2000687.

[22] Q. Wu, H. Ning, Q. Jiang, P. Han, M. Lin, G. Zhang, J. Chen, H. Chen, S. Zeng, J. Gao, J. Liu, F. He, *Energy Environ. Sci.,* 2021, DOI: 10.1039/D1EE01336J.